Rice University

Observation of antiferromagnetic correlations in the Fermi-Hubbard model

by

Pedro M Duarte

A Thesis Submitted
in Partial Fulfillment of the
Requirements for the Degree

Doctor of Philosophy

Approved, Thesis Committee:

Randall G. Hulet, *Chair*
Fayez Sarofim Professor of Physics and Astronomy

Thomas. C. Killian
Professor of Physics and Astronomy

Somebody Else
Professor of Physics and Astronomy

Houston, Texas
December 2012

Abstract

Observation of antiferromagnetic correlations in the Fermi-Hubbard model

by

Pedro M Duarte

Abstract goes here.

Acknowledgments

Acknowledgments go here.

Table of Contents

1.1 Motivation: Strongly correlated materials

Most of uur experiences in the physical world can, in principle, be explained by considering the description of the collections of positively charged nuclei and negatively charged electrons that make up ordinary matter. From high to low energy this includes: neutral plasmas, free atoms and molecules, atoms and molecules that have condensed into liquid or glassy phases or crystallized to form solids. At lower energies more exotic phenomena take place, starting with magnetism and going further to superfluidity, superconductivity and the novel examples of modern condensed matter physics such as the fractional quantum Hall effect, heavy electrons, high-temperature superconductors and topological insulators.

In principle, the correct description of all the above phenomena is contained in the Schrödinger equation for the interacting system of electrons and nuclei, where the interaction is given by the Coulomb potential. In practice, we know that even though stating the equation is easy, there is not sufficient computing power available in the world to solve it for systems of more than just a few particles. Xiao-Gang Wen, in the introduction to his book [1], points out that back in the 80's a computer with 32 MB of RAM could solve a system of 11 interacting electrons. In the 2000's, while computing power has increased more than 100 times, this allows for the addition of only two more electrons to the system.

Despite the above, the use of the Schrödinger equation and perturbation theory for the description of systems of electrons and nuclei has been very successful over the past century. The most prominent example of this success is our understanding of semiconductors, which are at the root of the electronic devices that permeate all aspects of our lives. The remarkable success of condensed matter physics can be traced back to the principle of adiabatic continuity [2]. This principle states that the low-energy excitations of an interacting system

are **non-interacting quasiparticles** which can be closely related to the actual particles that form the interacting system. This last sentence may sound confusing, but think about a hole in the valence band of a semiconductor. The hole corresponds to a collective arrangement of all the electrons in the system, but we typically do not think about it that way. The hole is a low energy excitation of the collection of electrons, and thus we think about it as a **quasiparticle**, with properties that are remarkably similar to those of a free electron albeit with a positive rather than a negative charge. The fact that an electron and a hole behave so similarly is not at all intuitive, especially if one stops to think about any effects due to the Coulomb interaction between electrons. However, adiabatic continuity guarantees that for practical purposes we can think of the hole simply as a positively charged electron.

The practical consequence of adiabatic continuity is that interactions seemingly do not play an important role in the low-energy description of the system. For this reason, the free electron model of Drude and Sommerfeld [3] is relatively successful in explaining electrical and thermal conductivity in metals, and also in explaining the Hall effect. In 1957, Landau formulated the theory of the Fermi-Liquid [4] and gave a solid basis to the notion of adiabatically connected quasiparticles. To this day, the Fermi-Liquid theory is the default starting point for the study of Fermi systems such as conventional metals, helium-3, and ultracold atomic Fermi gases.

But, just as Fermi-Liquid theory is celebrated for its success, it is also known for the phenomena that it fails to explain. Starting in the mid 70's and going through the 80's, the discoveries of heavy electron superconductivity [5, 6], the fractional quantum Hall effect [7, 8], and high-temperature superconductors [9] sparked a revolution in condensed matter physics [10]. These materials, in which the electron behavior cannot be described effectively in terms of non-interacting electron-like quasiparticles came to be known as **strongly correlated materials**. Strongly correlated materials, and the concept of emergence, introduced by P.W. Anderson in his famous essay "More is Different" [11], are at the center of modern condensed matter physics.

The behavior of strongly correlated materials is emergent because the low-energy excitations of the system bear no resemblance to its constituent particles. This disconnect should not be so surprising, after all we are familiar with this definition of emergence whenever a system undergoes a phase transition. For example, when a liquid cools down to form a crystalline solid, continuous translational symmetry is broken. By going across the liquid-to-solid phase transition, adiabatic continuity is violated; nevertheless, it is easy to mathematically identify the low energy excitations of the system and ascribe them the character of quasiparticles. In the case of the crystalline solid this involves finding the normal modes of a set of coupled oscillators; the normal modes are the quasiparticles known as phonons. Phonons are emergent because they bear no direct resemblance to the constituent ions that form the crystal lattice.

Strongly correlated materials are examples of emergent phenomena in which the origin and properties of the low-energy excitations are not as straightforward as those of phonons in a crystalline solid. The fractional quantum Hall state, in which the quasiparticles carry a rational fraction of the electron charge serves to illustrate this point. The strong interactions between the electrons in the quantum Hall system (electrons confined in a plane in the presence of a very high magnetic field) make the problem intractable from the perturbative point of view and thus **the connection between the microscopic degrees of freedom and the collective low-energy excitations is very difficult to establish**; certainly not as easy as the connection between small displacements of ions about their equilibrium points in a crystal lattice and the collective phonon modes. It was Laughlin's insight that led him to postulate the correct wavefunction for the quantum Hall state [8], but the microscopic origin of the state is still under debate.

The challenge posed by strongly correlated materials has led to great discoveries in condensed matter physics, such as the concepts of topological order [12] and quantum criticality [13, 14], but also many questions remain unanswered. Furthermore, the problem of strongly correlated materials is only scratching the surface of what is possible and what remains to be discovered. New materials are being synthesized constantly. Among the

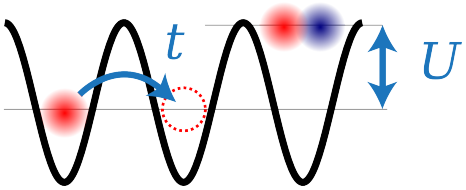

Figure 1.1: Illustration of the Hubbard model

myriad of possible materials and compounds yet to be explored by materials scientists, one can only expect that there will be new states of matter to be found; states with technological implications that will revolutionize life on earth.

1.2 Quantum simulations with ultracold atoms

We have seen that, even though the Schrödinger equation in principle contains a full description of a solid, its solution is practically impossible to compute using a classical computer due to the large amount of memory required to represent a many-body quantum state. The approach in condensed matter theory, rather than directly aim to solve the complete Schrödinger equation, is to introduce simplified effective models, which should capture the essential features of the system under study. The solution of the effective model leads to an understanding of the low-energy excitations of the system and gives clues to their microscopic origin.

The Hubbard model, formulated half a century ago [15] contains only the essential ingredients necessary to describe the behavior of strongly interacting electrons moving in a periodic lattice. It describes electrons that can hop between sites in a lattice (with probability amplitude t) , and which acquire an interaction energy (U) when two electrons are on the same site, see Figure 1.1. The Hubbard model is an extension of the tight-binding model, with the interactions between electrons incorporated as the on-site energy U. After its inception, it was shortly realized [16] that the model could explain the Mott metal-insulator transition, which was observed in the transition metal oxides even though conventional band theory predicted them to be conductors. Beyond its early success, the Hubbard model is now the quintessential model for strongly correlated systems. It is widely accepted as the

most viable candidate to explain high-T_c superconductors from first principles. Despite this fact, its exact solution in more than one dimension has evaded theorists for more than four decades [17].

It is at this point that ultracold atoms enter the picture. It turns out that ultracold atoms in an optical lattice provide a faithful realization of the Hubbard model [18], thus the properties exhibited by the collection of atoms are in fact the solutions of the model. In this way, such systems can be used to map the phase diagram of the Hubbard model in what is known as **quantum simulation**, an idea that was first proposed by Richard Feynman in 1982 [19].

In a seminal paper [18], Jaksch and collaborators showed that Bose-Einstein condensates of atoms loaded into optical lattices could be used as simulators of the Bose-Hubbard model. A few years later, the superfluid (SF) to Mott insulator (MI) phase transition, the hallmark of the Bose-Hubbard model, was realized experimentally [20], and several detailed studies of this system have followed since then [21–25]. For bosonic systems the properties of the ground state are well understood theoretically [26–28]; however, experiments of atoms in lattices are starting to shed light into the dynamics of these systems [29], which are more difficult to address for theorists.

Despite the remarkable advances with bosonic systems, the ultimate goal of quantum simulation with ultracold atoms is to find the ground states of theoretically intractable fermionic models, to see if these models can reproduce the measured properties of strongly correlated electron systems. In this prescription for quantum simulation, the subject of most interest is whether or not the Hubbard model can exhibit a d-wave superfluid state which would validate it as the prime model for high-T_c superconductors [30, 31]. In pursuit of this goal, experiments have realized the Hubbard model with spin mixtures of fermionic atoms, where two hyperfine levels of the atomic ground state play the role of spin-up and spin-down states of the spin-$\frac{1}{2}$ electrons in real compounds.

In these experiments, a quantum degenerate spin-mixture of fermionic atoms is prepared

in a harmonic potential and then transferred adiabatically into an optical lattice potential. The lattice depth and the contact interactions between the atoms, which together set the values for the Hubbard parameters t and U, can be controlled almost at will by the experimenter. The tunneling rate t is controlled by adjusting the intensity of the lattice lasers. The interaction strength U is controlled by setting the external magnetic field and making use of a magnetically tunable Feshbach resonance, which offers the possibility of realizing non-interacting samples, or samples with, arbitrarily, large attractive or repulsive interactions[1]. These unprecedented control over the system parameters has allowed the realization of band insulating states [33] and Mott insulating states [34, 35] with spin-mixtures of ultracold fermionic atoms. However, the possibility of exploring the strongly correlated phases of the Hubbard model has not yet been realized because the required temperatures are out of reach for current experiments.

1.3 Quantum magnetism with ultracold atoms

Even though temperatures as low as $T \simeq 0.04\,T_F$ can be reached with ultracold Fermi gases in a harmonic trap, these temperatures are not low enough to allow exploration of the strongly correlated phases of the Hubbard model. To get an idea of the temperature scales involved, we will examine a qualitative temperature-doping phase diagram, which can be obtained experimentally for the cuprate high-T_c superconductors[2], see Fig. 1.2.

The qualitative phase diagram shows that the cuprates exhibit various interesting phases besides the superconducting (SC) dome at intermediate doping. Most importantly, the undoped parent compound is an antiferromagnetic (AFM) Mott insulator with a Néel ordering temperature that is higher than any value of the critical temperature T_c along the SC dome.

The onset of AFM ordering in the cuprate parent compounds is driven by the magnetic exchange interaction [40], where a pair of spins can lower their energy if they can tunnel

[1] In practice it is observed that, for some values of the interaction strength, significant three-body losses and the associated heating rates prevent studying the equilibrium physics of the quantum gas [32].

[2] See [36] for a review of cuprate superconductors, [37] for a study of the onset of superconductivity at optimal hole-doping, [38] for the phase diagram of hole-doped cuprate superconductors and [39] for a more accessible report on the subject.

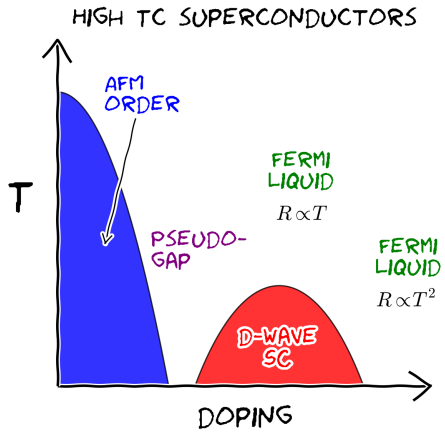

Figure 1.2: Cartoon phase diagram for cuprate high-T_C superconductors. The anitiferromagnetic insulator (AFM) and the Fermi liquid with quadratic resistivity are well understood by theory, however the strange Fermi liquid with linear resistivity and the interplay between the pseudogap regime and the superconducting dome are issues still under debate [39].

virtually to the neighboring site. For a single band model, the Pauli exclusion principle dictates that this is only possible if neighboring sites have opposing spins, as in the Néel AFM state. The Néel temperature T_N is then on the order of the exchange energy $4t^2/U$, which is the second-order correction (due to virtual tunneling) to the ground state energy of a two-site model where the interaction U is treated as a perturbation. The undoped parent compounds, at temperatures several times larger than T_N, will be Mott insulators with exactly one electron per lattice site but without any kind of spin ordering. As T_N is approached, AFM correlations between the spins start to develop.

To put some estimates on the values of T_N and T_c, let's consider the most common high-T_c superconductor [41], $YBa_2Cu_3O_{6+x}$, usually referred to as YBCO. The critical temperature for YBCO can be as large as $T_c \simeq 93$ K, obtained for optimal hole-doping [42]. In the absence of doping, the YBCO parent compound is antiferromagnetic with a Néel temperature $T_N \simeq 500K$ [43]. The Fermi energy for YBCO is on the order of ~ 4 eV [44], which corresponds to $\sim$ 40000 K. In units of the Fermi temperature T_F, we have $T_C \simeq 0.002\,T_F$, and $T_N \simeq 0.012\,T_F$.

We immediately see that, in units of T_F, the relevant temperatures for d-wave super-

conductivity and for antiferromagnetism are both higher than state-of-the-art temperatures for ultracold fermionic atoms. The Mott insulator state (without spin ordering) was first realized with fermionic atoms in a simple cubic lattice in 2008 [34, 35]. Immediately after that, the race started to see which group could be the first to observe the AFM state and take the next step in the roadmap of quantum simulation.

Recently in 2013, the Esslinger group, at ETH Zürich, has demonstrated the use of a dimerized optical lattice to measure the nearest-neighbor spin correlations that start to develop, as a consequence of the exchange interaction, at temperatures a few times larger than the Néel temperature for AFM ordering [45]. They observe significant spin-spin correlations in arrays of 1D chains and they can detect the spin-spin correlations that form on the approach to AFM order in a simple cubic lattice. Prior to the work of the Esslinger group, the Bloch group used a similar optical super-lattice to study exchange interactions with bosons in isolated double-wells [46] and isolated four-site plaquettes [47].

Other experiments have realized AFM states in engineering Ising hamiltonians, using trapped ions [48, 49], or by mapping motional degrees of freedom to effective Ising models [50, 51]. In Ising type models, the magnetic coupling (anti or ferromagnetic) is put in by hand in the Hamiltonian, and thus they realize what is referred to as classical magnetism. In the Hubbard model, on the other hand, magnetism arises from the exchange interaction, like it does in condensed matter systems such as the transition metal oxides or the cuprate parent compounds. Realizations of classical magnetism are excellent systems to study magnetic frustration, or the dynamics of quenching the system across a phase-transition [52]. Systems of trapped ions can help understand models with long range interactions [53], and also emerge as good candidates to realize universal quantum computers [49]. However, despite their advantages in other areas, these systems do not directly address the long-standing open question of superconductivity in the Hubbard model.

Seven years ago, the Hulet lab started an experiment to study strongly correlated matter using ultracold atoms in optical lattices; our main goal being the achievement of tempera-

tures below the Néel transition temperature. The Néel state in the Hubbard model, besides being the natural stepping stone in the quest to simulating strongly correlated systems, offers the added benefit that is a state that is well understood by theory [54, 55]. The ability to compare experimental results with theory offers a test bed for quantum simulation and also a way to establish absolute thermometry for ultracold atoms in optical lattices, which is another major challenge in this field [56].

1.4 This thesis

Over the course of this work we have used a compensated lattice potential, which allows excellent control over the density distribution of the atoms in the lattice. The compensated lattice also helps mitigate heating of the atoms as they are loaded into the lattice and has allowed us to reach temperatures as low as 1.4 T_N, which is a factor of 2 colder than previous experiments [57]. We measure the temperature of the atoms in the lattice using Bragg scattering of light off of the magnetic sublattices that start forming on the approach to the Néel transition. This technique has been discussed before [58] but only until now implemented. A very important aspect of our work is the comparison to *ab initio* numerical simulations of the Hubbard model. We have used results from determinantal quantum Monte Carlo (DQMC) [54] and from numerical linked-cluster expansion (NLCE) [59] calculations, along with the local density approximation to establish the link between light scattering and absolute thermometry of the sample.

1.4.1 Outline

In this subsection I plan to give a small overview of what is covered in each chapter, but first I have to go ahead and write the chapters.

In this chapter we consider the description of cold atoms in an optical lattice potential. Second quantization is introduced, and the many-body Hubbard hamiltonian is derived, thus making the case for ultracold atoms as a nearly ideal realization of the Hubbard model. We discuss the requirements necessary for the ultracold atom system to be well described by a single band Hubbard model.

2.1 One-dimensional optical lattice potential

The contents of this section follow the derivation found in § IV.A of the review article by Morsch and Oberthaler. [60]. The hamiltonian for an atom moving in a one-dimensional (1D) sinusoidal potential, such as that produced by an optical lattice, is

$$H_{\text{single,1D}} = -\frac{\hbar^2}{2m}\frac{\partial^2}{\partial x^2} + V_0 \sin^2(kx) \tag{2.1}$$

where $k = 2\pi/\lambda$, and λ is the wavelength of the lattice laser. The lattice depth V_0 is naturally expressed in units of the recoil energy: $E_r = \frac{\hbar^2 k^2}{2m}$. Defining $v_0 = V_0/E_r$ the hamiltonian reduces to

$$\begin{aligned} H_{\text{single,1D}} &= -\frac{1}{k^2}\frac{\partial^2}{\partial x^2} + v_0 \sin^2(kx) \\ &= -\frac{1}{k^2}\frac{\partial^2}{\partial x^2} + \frac{v_0}{4}(2 - e^{2ikx} - e^{-2ikx}) \end{aligned} \tag{2.2}$$

The solutions to the time independent Schrödinger equation for this hamiltonian are Bloch states, which are labeled by their quasimomentum q and their band index n, and can be written in general form as

$$\psi_q^n(x) = e^{iqx} \sum_{l \in \mathbb{Z}} c_{ql}^n e^{ilGx} \tag{2.3}$$

The lattice translation invariant function that accompanies e^{iqx} in a Bloch state has been written here, with no loss of generality, as a sum of plane waves with momenta lG, where

l is an integer, $G = 2k = 2\pi/a$ is the magnitude of the primitive vector of the reciprocal lattice, and $a = \lambda/2$ is the lattice spacing.

Acting with the hamiltonian on the Bloch states and then rearranging some of the terms in the infinite sum, we get

$$\begin{aligned} H_{\text{single,1D}}\psi_q(x) &= \sum_l \left[(q/k+2l)^2 + \frac{v_0}{4}(2 - e^{2ikx} - e^{-2ikx})\right] c_{ql}^n e^{iqx+il2kx} \\ &= \sum_l \left[\left((q/k+2l)^2 + \frac{v_0}{2}\right) c_{ql}^n - \frac{v_0}{4}c_{q,l-1}^n - \frac{v_0}{4}c_{q,l+1}^n\right] e^{iqx+il2kx} \end{aligned} \tag{2.4}$$

The quasimomentum is restricted to the first Brillouin zone, which can be taken to be $[-\frac{\pi}{a}, \frac{\pi}{a})$. The natural unit for the quasimomentum is $2\pi/a$ or $2k$. Defining $q' = q/(2k)$, we can then write the time-independent Schrödinger equation as

$$\left((2q'+2l)^2 + \frac{V_0}{2}\right) c_{ql}^n - \frac{V_0}{4}c_{q,l-1}^n - \frac{V_0}{4}c_{q,l+1}^n = E_q c_{ql}^n \tag{2.5}$$

We then have an infinite linear system of equations which determines the c_{ql}^n. For our practical purposes we truncate the set of equations such that $|l| < \mathcal{N}$. The resulting equations can be written in matrix form, for example if we select $\mathcal{N} = 2$

$$\begin{bmatrix} \frac{1}{2}V_0+4(q-2)^2 & -\frac{1}{4}V_0 & 0 & 0 & 0 \\ -\frac{1}{4}V_0 & \frac{1}{2}V_0+4(q-1)^2 & -\frac{1}{4}V_0 & 0 & 0 \\ 0 & -\frac{1}{4}V_0 & \frac{1}{2}V_0+4q^2 & -\frac{1}{4}V_0 & 0 \\ 0 & 0 & -\frac{1}{4}V_0 & \frac{1}{2}V_0+4(q+1)^2 & -\frac{1}{4}V_0 \\ 0 & 0 & 0 & -\frac{1}{4}V_0 & \frac{1}{2}V_0+4(q+2)^2 \end{bmatrix} \cdot \begin{bmatrix} c_{q,-2}^n \\ c_{q,-1}^n \\ c_{q,0}^n \\ c_{q,1}^n \\ c_{q,2}^n \end{bmatrix} = E_q^n \begin{bmatrix} c_{q,-2}^n \\ c_{q,-1}^n \\ c_{q,0}^n \\ c_{q,1}^n \\ c_{q,2}^n \end{bmatrix} \tag{2.6}$$

These equations can be solved to obtain the eigenvectors c_{ql}^n and the eigenvalues E_q^n. In the numerical solution that we implemented we truncated the infinite set at $\mathcal{N} = 5$. To accurately obtain the dispersion relationship for the n^{th} band you need $\mathcal{N} \geq n + 1$.

2.1.1 Band structure

The eigenvalues obtained from the solutions to Eq. 2.6 correspond to the energies E_q^n as a function of quasimomentum q and band index n, and is referred to as the band structure. We show it for a 1D lattice as a function of q in Fig. 2.1, and also as a function of lattice depth in Fig. 2.2

The time independent Schrödinger equation for the hamiltonian in Eq. 2.1, can also be solved using Mathieu functions. One can then calculate the band structure by using the

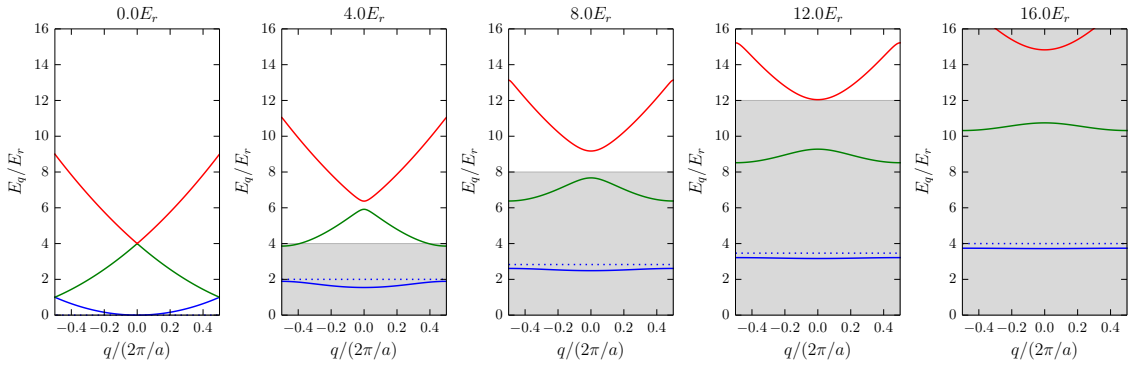

Figure 2.1: Band structure in a 1D optical lattice. The depth of the lattice is indicated by the shaded area, and the energy of the harmonic oscillator ground state in a single lattice site is shown as a dotted line.

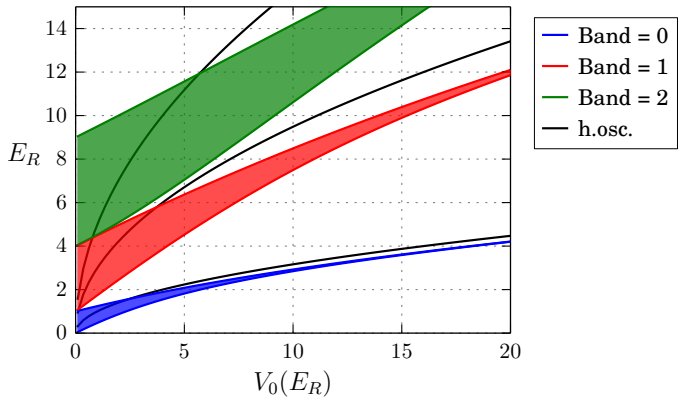

Figure 2.2: Band structure in a 1D optical lattice. Each band is indicated by the colored area, the harmonic oscillator states in an isolated lattice site are shown as black lines.

known properties of the Mathieu functions, which are available on tables or as functions in some software packages (e.g. Mathematica), see for instance the treatment in [61].

2.1.2 Eigenstates

For each energy eigenvalue we have an associated eigenstate which is defined in terms of the c_{ql}^n by Eq. 2.3. Typically, numerical diagonalization routines return the normalized eigenvectors of the matrix in question, and for us this means that the coefficients c_{ql}^n will satisfy

$$\sum_l |c_{ql}^n|^2 = 1 \tag{2.7}$$

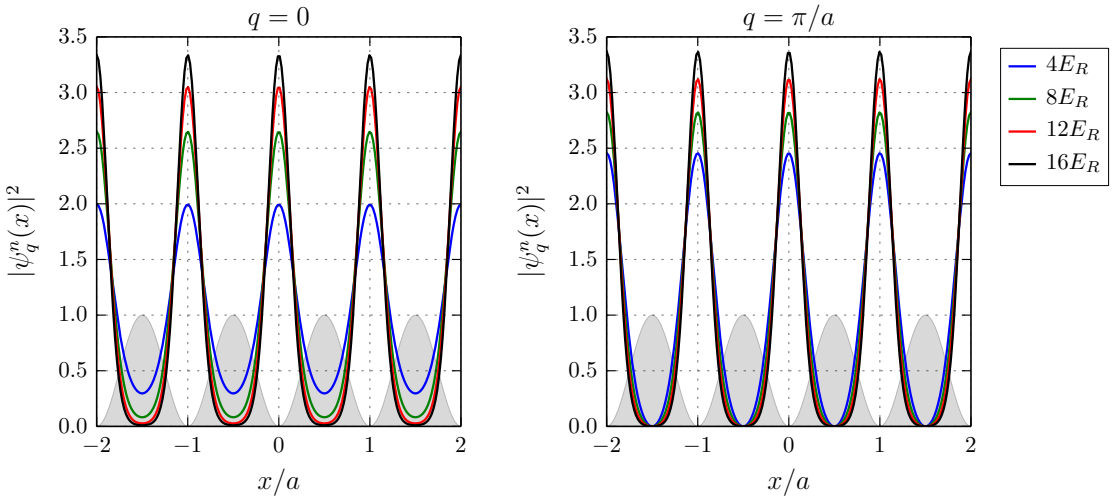

Figure 2.3: Eigenstates of the Hamiltonian in a 1D optical lattice shown for $q = 0$ (left) and $q = \pi/a$ (right) for various lattice depths. The states are normalized so that the integral of the probability density over one lattice site is equal to one. The gray shaded region is shown to indicate the variation of the lattice potential.

This has the implication that the states obtained from Eq. 2.3 will be normalized over a lattice site. In Fig. 2.3. we show the probability density for a lowest band eigenstate as a function of position in the lattice for various lattice depths. One can see how, as the lattice gets deeper, the state becomes more localized around the center of each lattice site.

2.1.3 Wannier states

It is useful to define a basis of states that are localized around a single lattice site. We will see later on that, when using such a basis, the hamiltonian for the Hubbard model takes its most familiar form. In a finite sized lattice with L sites, the localized state centered around the j^{th} site(at x_j) can be constructed as the following superposition of eigenstates of the hamiltonian[1]:

$$w^n(x - x_j) = \frac{1}{L} \sum_q e^{-iq2\pi x_j} \psi_q^n(x) \tag{2.8}$$

[1] In some treatments (for instance [62]) the Wannier function is defined with a normalization factor of $\sqrt{L}$ rather than L as shown here. This is considering eigenfunctions $\psi_q^n(x)$ which are normalized when integrating over the full extent in the lattice. We stick to the L normalization factor, without the square root, since the eigenfunctions that are obtained numerically come out normalized over a lattice site, as was explained in the previous section.

Here the sum runs over the set of quasimomenta $q \in \left\{ \frac{2\pi u}{aL} \mid u \in \{0, 1, \dots L-1\} \right\}$. Inserting the expansion of $\psi_q^n(x)$ in plane waves into the definition of the Wannier state we obtain

$$w^n(x - x_j) \equiv w_j^n(x) = \frac{1}{L} \sum_q \sum_{l \in \mathbb{Z}} c_{ql}^n e^{-i2\pi q x_j} e^{i2\pi(q+l)x} \tag{2.9}$$

We will set $x_j = 0$ for the calculation of the Wannier function, Wannier states centered at different lattice sites can be obtained by translation of the $x_j = 0$ solution.

$$w_0^n(x) = \frac{1}{L} \sum_q \sum_{l \in \mathbb{Z}} c_{ql}^n e^{i2\pi(q+l)x} \tag{2.10}$$

Since the hamiltonian commutes with the parity operator, it is required that $\psi_q^n(-x) = \pm\psi_q^n(x)$, which implies that $c_{ql}^n = \pm c_{pl'}^n$ if $(q + l) = -(p + l')$. Using this symmetry, the Wannier state can be written as

$$w_0^n(x) = \frac{1}{L} \left(c_{00}^n + \sum_{q>0} \sum_{l>0} c_{ql}^n \left[e^{i2\pi(q+l)x} \pm e^{-i2\pi(q+l)x} \right] \right) \tag{2.11}$$

It is shown in [63] that the maximally localized Wannier states are obtained if the plus sign is chosen for even bands and the minus sign is chosen for odd bands. So, the $x_j = 0$ Wannier state is symmetric for the even bands and antisymmetric for the odd bands.

$$w_0^n(x) = \frac{c_{00}^n}{L} + \frac{2}{L} \sum_{q>0} \sum_{l>0} c_{ql}^n \begin{cases} \cos[2\pi(q+l)x] & \text{if } n \text{ even} \\ \sin[2\pi(q+l)x] & \text{if } n \text{ odd} \end{cases} \tag{2.12}$$

After defining the way to construct the Wannier states starting from the c_{ql}^n, we can now proceed to add up the plane waves to obtain the states, as shown in Fig. 2.4 for various lattice depths. As the lattice depth is increased, the Wannier states become more localized, which leads to less overlap between states in adjacent sites, and results in a reduction of the probability amplitude for a particle to tunnel from one site to the neighboring one. More localized states also imply that the on-site interaction will be larger, since, on average, two particles in the same site will be closer to each other.

We also show, in Fig. 2.5, the Wannier functions for the first three bands in a $4E_R$ lattice.

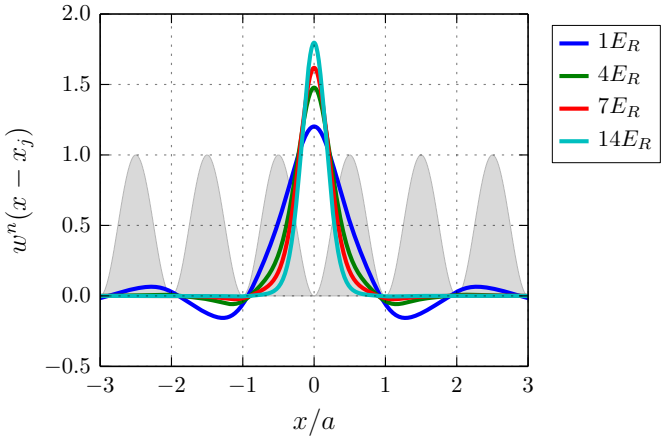

Figure 2.4: Wannier states localized at $x_j = 0$ in a 1D optical lattice for various lattice depths. The gray shaded region is shown to indicate the spatial variation of the lattice potential.

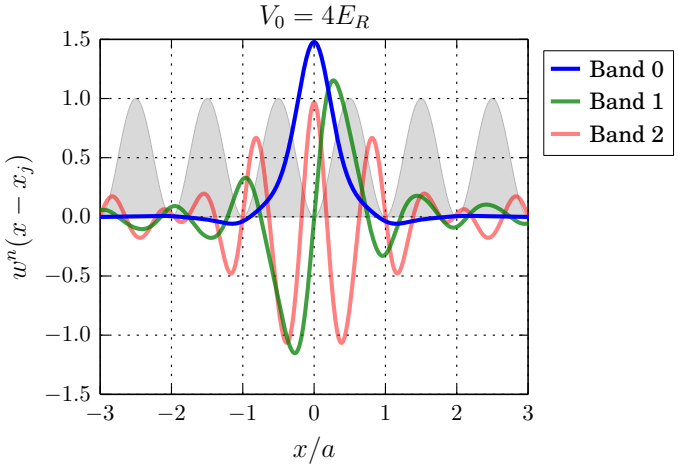

Figure 2.5: Wannier states localized at $x_j = 0$ in a $4E_R$ 1D optical lattice for the first three energy bands. The gray shaded region is shown to indicate the spatial variation of the lattice potential.

2.2 Three-dimensional optical lattice potential

The hamiltonian for an atom moving in a 3D lattice can be separated in the three spatial coordinates. So we can use the solutions that were obtained in the previous section for the 1D lattice and obtain the band structure and the Wannier states for the 3D lattice. The 3D band structure is shown in Fig. 2.6.

The Wannier states in a 3D lattice are simply products of the Wannier states in each of

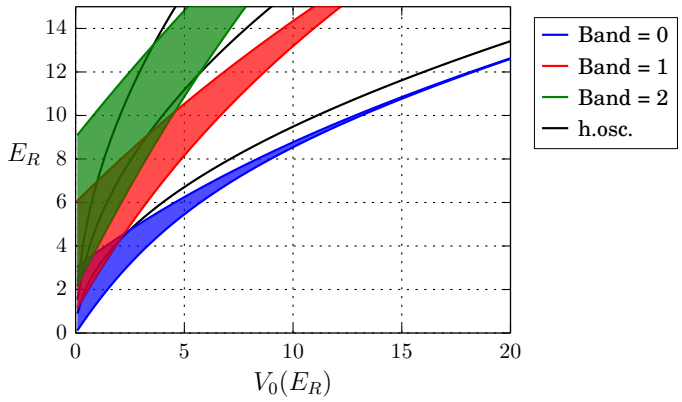

Figure 2.6: Band structure in a 3D optical lattice. Each band is indicated by the colored area, the harmonic oscillator states in an isolated lattice site are shown as black lines.

the three spatial coordinates. They are defined as

$$w^n(\boldsymbol{r} - \boldsymbol{r}_j) = \frac{1}{L^3} \sum_{\boldsymbol{q}} e^{-i\boldsymbol{q}\cdot\boldsymbol{r}_j} \prod_{u=x,y,z} \psi_{q_u}^{n_u}(u) \tag{2.13}$$

where L^3 is the total number of sites in the lattice.

2.3 Hubbard hamiltonian

The many-body Hubbard hamiltonian is

$$H = -t \sum_{\langle ij\rangle,\sigma} a_{i\sigma}^\dagger a_{j\sigma} + U \sum_i n_{i\uparrow} n_{i\downarrow} \tag{2.14}$$

where i, j are indices that run over lattice sites, $\langle ij\rangle$ denotes nearest-neighbors, and σ denotes the spin state of the particles. The particle creation and annihilation operators, $a_{j\sigma}$ and $a_{i\sigma}^\dagger$, along with the number operator $n_{i\sigma}$ arise naturally in the second quantization formalism. In what follows, we will see how to obtain this many-body form, starting from the first quantized version of the hamiltonian for a system of N particles moving in a periodic lattice.

The hamiltonian for a single atom in a 3D optical lattice is given by

$$H_{\text{single,3D}} = -\frac{\hbar^2}{2m}\left(\frac{\partial^2}{\partial x^2} + \frac{\partial^2}{\partial y^2} + \frac{\partial^2}{\partial z^2}\right) + V_0\left(\cos^2(kx) + \cos^2(ky) + \cos^2(kz)\right) \tag{2.15}$$

and when N particles are considered, along with their interactions the hamiltonian takes a more complicated form

$$\begin{aligned} H =& \sum_{l}^{N}\left[-\frac{\hbar^2}{2m}\left(\frac{\partial^2}{\partial x_l^2}+\frac{\partial^2}{\partial y_l^2}+\frac{\partial^2}{\partial z_l^2}\right)+V_0\left(\cos^2(kx_l)+\cos^2(ky_l)+\cos^2(kz_l)\right)\right] \\ &+\frac{1}{2}\sum_{l,n,l\neq n}^{N} V_{\text{int}}(\boldsymbol{r}_l,\boldsymbol{r}_n) \\ \equiv& H_0+H_{\text{int}} \end{aligned} \tag{2.16}$$

where the particles are labeled by indices l,n and V_{int} is the potential energy of interaction between two particles. In the last line we have defined a more concise notation that splits the Hamiltonian into the non-interacting (H_0) and interacting (H_{int}) parts. Solving this problem is a daunting task primarily for two reasons:

1. The Bose or Fermi statistics of the identical particles under consideration require the solutions to be symmetrized or antisymmetrized products of single-particle wavefunctions.

2. The interactions between the particles prevent a straightforward reformulation of the problem as a collection of easier-to-solve single particle hamiltonians.

The formalism of many-body theory encapsulates a series of methods to deal with the two issues mentioned above. First, the reformulation of the Schrodinger equation in the language of second quantization provides the advantage that the statistics are automatically taken into account by the notation, so one can essentially forget about the the (anti)symmetrization of the many-particle wave functions. The small price to pay is that one needs to be very careful and consistent about the order in which operators show up in the notation, since the symmetry properties of the resulting states are contained in the commutation relations defined between the operators. Furthermore, second quantization makes it easy to consider the extended Hilbert space where the number of particles is not fixed, known as the Fock space.

For weak interactions, many-body theory provides a solution to the problem in terms of perturbation expansions for the physical quantities of interest. The theoretical formalism also reduces most of the important physical quantities in terms of certain matrix elements (Green's functions) which allows the user to concentrate on obtaining such matrix elements which serve as a starting point for the exploration of the properties of any system. The complication arises when the interactions are not weak, and the perturbative approach of the many-body formalism breaks down.

2.3.1 Second quantization

The contents of this section comprise a short summary of the treatment in the books by Fetter and Walecka [64] and Schwabl [65].

Let us start with a complete orthonormal set of single particle states $\{|i\rangle\} \equiv \{|1\rangle, |2\rangle, \ldots\}$, using these states we can write the basis states for the N-particle system as

$$|i_1, \ldots i_\alpha, \ldots i_N\rangle \equiv |i_1\rangle_1 \ldots |i_\alpha\rangle_\alpha \ldots |i_N\rangle_N \ , \tag{2.17}$$

which represents a state in which particle 1 is in state $i_1 \in \{|i\rangle\}$, particle α is in state i_α and so on. These product states are not eigenstates of the permutation operator P_{ij} which interchanges particles i and j. However, starting from the product states we can obtain the completely (anti)symmetrized basis states for bosons (fermions), which are eigenstates of any possible permutation of the particle labels.

For bosons, the normalized completely symmetric states are

$$|n_1, n_2, \ldots\rangle = \frac{1}{\sqrt{N! n_1! n_2! \ldots}} \sum_P P|i_1, i_2, \ldots i_N\rangle \tag{2.18}$$

where the P's are elements of the permutation group[2] In this expression, n_i is the number of times that the state $|i\rangle$ occurs among the N particles, also called the occupation number of state $|i\rangle$. The sum of all occupation numbers n_i must equal the total number of particles, but otherwise there is no restriction in the occupation number for bosons.

[2]For N particles there are $N!$ possible permutations and thus $N!$ elements in the permutation group.

For fermions the normalized completely antisymmetric states have an extra factor $(-1)^P$, which denotes the parity of the permuatation P. They can be written in the form of Slater determinants:

$$\begin{aligned} |n_1, n_2, \ldots\rangle =& \frac{1}{\sqrt{N!}} \sum_P (-1)^P P |i_1, i_2, \ldots i_N\rangle \\ =& \frac{1}{\sqrt{N!}} \begin{vmatrix} |i_1\rangle_1 & |i_1\rangle_2 & \cdots & |i_1\rangle_N \\ \vdots & \vdots & \ddots & \vdots \\ |i_N\rangle_1 & |i_N\rangle_2 & \cdots & |i_N\rangle_N \end{vmatrix} \end{aligned} \tag{2.19}$$

If a single particle state appears more than once in the product state, the resulting totally antisymmetric state is zero, i.e. the occupation numbers n_i can only take the values 0 or 1, a consequence of the Pauli exclusion principle.

For bosons (fermions), we can combine the (anti)symmetric states for $N = 0, 1, 2, \ldots$ particles to obtain a complete orthonormal set of states for arbitrary particle number. This "number states" are the basis of the Fock space.

We will concentrate in the case of fermions, and define the creation operators such that the number state can be written as

$$|n_1, n_2, \ldots\rangle = \left(a_1^\dagger\right)^{n_1} \left(a_2^\dagger\right)^{n_2} \ldots |0\rangle \tag{2.20}$$

where $|0\rangle$ is the vacuum state, in which there are no particles. By definition, the number state is completely antisymmetric, but what does this imply for the creation operators? Going back to Eq. 2.19, which defines the number states, we see that the sign of the number state depends on the particular ordering of the single particle states in the Slater determinant. Suppose $n_1 = n_2 = 1$, changing the labels on states 1 and 2 corresponds to exchanging two rows in the Slater determinant and thus a minus sign comes out:

$$\left(a_2^\dagger\right)^{n_2} \left(a_1^\dagger\right)^{n_1} \ldots |0\rangle = -|n_1, n_2, \ldots\rangle \tag{2.21}$$

Comparing with Eq. 2.20 we notice that the creation operators must then satisfy the following anticommutation relation

$$a_1^\dagger a_2^\dagger + a_2^\dagger a_1^\dagger \equiv \left\{a_1^\dagger, a_2^\dagger\right\} = 0 \tag{2.22}$$

Notice that this anticommutation relation implies $\left(a_i^\dagger\right)^2 = 0$, which is yet another manifestation of the Pauli exclusion principle.

When dealing with Fermions, one must decide first on a particular ordering of the single particle states and then stick to it, noticing that to produce the number states (without a minus sign) all the creation operators must be applied to the vacuum state in the chosen order. The action of a creation operator on a number state is

$$a_i^\dagger|\ldots, n_i, \ldots\rangle = (-1)^{\sum_{k<i} n_k}|\ldots, n_i + 1, \ldots\rangle \tag{2.23}$$

where the factor $(-1)^{\sum_{k<i} n_k}$ takes care of the number of anticommutations needed to place the $a_i^\dagger$ operator in the correct position. The action of the fermion annihilation operators can be inferred by taking the adjoint of Eq. 2.23. One can then obtain all of the anticommutation rules for fermions:

$$\{a_i, a_j\} = 0 \qquad \left\{a_i^\dagger, a_j^\dagger\right\} = 0 \qquad \left\{a_i, a_j^\dagger\right\} = \delta_{ij} \tag{2.24}$$

2.3.2 Operators in second quantization

So far two great leaps have been taken:

1. We have swept antisymmetrization under the rug by introducing the number states, defined from the vacuum in terms of creation operators which satisfy the Fermi anticommutation rules.

2. We started from an N particle hamiltonian, but we have now defined number states that can handle the description of systems with an arbitrary number of particles

The two ideas mentioned are related to the states used to describe the system, now we will turn to the problem of the observables and see how they are handled in the second quantization.

Let us consider the sum $\sum_\alpha |i\rangle_\alpha\langle j|_\alpha$ where $|i\rangle$ and $|j\rangle$ are single particle states, and α runs over all particles in the system. We apply the sum to the number states using the

definition in Eq. 2.19:

$$\left(\sum_\alpha |i\rangle_\alpha\langle j|_\alpha\right)|n_1,n_2,\ldots\rangle = \frac{1}{\sqrt{N!}}\sum_P(-1)^P P\left(\sum_\alpha |i\rangle_\alpha\langle j|_\alpha|i_1,i_2,\ldots i_N\rangle\right) \tag{2.25}$$

For the term in the right not to vanish, the initial number state must have a particle in state $|j\rangle$, i.e. it must have $n_j = 1$. Also, n_i must be $n_i = 0$, or else the completely antisymmetric state will vanish. If the particle initially in state $|j\rangle$ is labeled as J we can write

$$\begin{aligned}\left(\sum_\alpha |i\rangle_\alpha\langle j|_\alpha\right)|n_1,n_2,\ldots\rangle =& \frac{1}{\sqrt{N!}}\sum_P(-1)^P P\left(|i_1\rangle_1|i_2\rangle_2\ldots \underbrace{|i\rangle_J}_{\text{instead of }|j\rangle_J}\ldots|i_N\rangle_N\right)\\ =& \frac{1}{\sqrt{N!}}\begin{vmatrix} |i_1\rangle_1 & |i_1\rangle_2 & \cdots & |i_1\rangle_N\\ \vdots & \vdots & & \vdots\\ |i\rangle_1 & |i\rangle_2 & \cdots & |i\rangle_N\\ \vdots & \vdots & & \vdots\\ |i_N\rangle_1 & |i_N\rangle_2 & \cdots & |i_N\rangle_N\end{vmatrix}\end{aligned} \tag{2.26}$$

In the determinant of the left, the state $|i\rangle$ appears in the j^{th} row, so a few rows need to be exchanged to put it in the correct place according to our sign convention for the number states:

$$\left(\sum_\alpha |i\rangle_\alpha\langle j|_\alpha\right)|n_1,n_2,\ldots\rangle = \begin{cases}(-1)^{\sum_{k<j}n_k+\sum_{k<i}n_k} & |n_1,n_2,\ldots,n_i+1,\ldots,n_j-1,\ldots\rangle \quad \text{if } i\le j,\\ (-1)^{\sum_{k<j}n_k+\sum_{k<i}n_k-1} & |n_1,n_2,\ldots,n_j-1,\ldots,n_i+1,\ldots\rangle \quad \text{if } i>j\end{cases} \tag{2.27}$$

Checking the definition of the creation and annihilation operators we obtain the important result

$$\left(\sum_\alpha |i\rangle_\alpha\langle j|_\alpha\right)|n_1,n_2,\ldots\rangle = a_i^\dagger a_j|n_1,n_2,\ldots\rangle \qquad \Rightarrow \qquad \sum_\alpha |i\rangle_\alpha\langle j|_\alpha = a_i^\dagger a_j \tag{2.28}$$

Now, consider an operator T that is a sum over single particle operators

$$T = \sum_\alpha t_\alpha \tag{2.29}$$

If we insert the completeness relation for the single particle states twice in this sum, we have

$$\begin{aligned} T =& \sum_{\alpha} \left(\sum_{i} |i\rangle_\alpha \langle i|_\alpha \right) t_\alpha \left(\sum_{j} |j\rangle_\alpha \langle j|_\alpha \right) \\ =& \sum_{ij} \langle i|t|j\rangle \sum_{\alpha} |i\rangle_\alpha \langle j|_\alpha \\ =& \sum_{ij} \langle i|t|j\rangle a_i^\dagger a_j \equiv \sum_{ij} t_{ij} a_i^\dagger a_j \end{aligned} \tag{2.30}$$

This is the other big leap provided by the second quantization: an operator that was written as a sum over particles becomes a sum of creation and annihilation operators. We will apply this prescription to the non-interacting part of the Hamiltonian for N particles moving in a lattice.

Operators like the potential energy, which are a sum over two-particle (or many-particle) operators, can be similarly expressed as sums of creation and annihilation operators [65]. For a two-body operator we have the expression

$$\begin{aligned} F =& \frac{1}{2} \sum_{\alpha \neq \beta} f(\boldsymbol{r}_\alpha, \boldsymbol{r}_\beta) \\ =& \frac{1}{2} \sum_{ijkm} \langle ij|f|km\rangle a_i^\dagger a_j^\dagger a_m a_k \end{aligned} \tag{2.31}$$

2.3.3 Second quantized Hubbard hamiltonian

The Hubbard hamiltonian in Eq. 2.16 is a sum of two single-particle operators and one two-particle operator. These are, respectively: the kinetic energy, the energy of the atoms in the lattice potential, and the interactions between the atoms. In this section we will express the Hubbard hamiltonian in second quantized form. As a single-particle basis we will use the Wannier states that were derived in Section. 2.1.3

Tunneling matrix element, t. H_0 is a single particle operator of the kind defined in Eq. 2.29:

$$H_0 = \sum_{l=1}^{N} H^l_{\text{single,3D}} \tag{2.32}$$

where

$$H^l_{\text{single,3D}} = -\frac{\hbar^2}{2m}\left(\frac{\partial^2}{\partial x_l^2}+\frac{\partial^2}{\partial y_l^2}+\frac{\partial^2}{\partial z_l^2}\right)+V_0\left(\cos^2(kx_l)+\cos^2(ky_l)+\cos^2(kz_l)\right) \tag{2.33}$$

It's second quantized form it can be written as

$$\begin{aligned} H_0 =& \sum_{ij}\langle i|H_{\text{single,3D}}|j\rangle a_i^\dagger a_j \\ \equiv& -\sum_{ij} t_{ij} a_i^\dagger a_j \end{aligned} \tag{2.34}$$

Note that the sign of t_{ij} was picked rather arbitrarily to follow the usual conventions. We now proceed to find the value of the matrix element t_{ij}. We use the definition of the Wannier states given in Eq. 2.13 to find

$$\begin{aligned} -t_{ij} =& \frac{1}{L^6}\int \mathrm{d}\boldsymbol{r}\ \sum_{\boldsymbol{q}'} e^{i\boldsymbol{q}'\cdot\boldsymbol{r}_i}\prod_{u'=x,y,z}\psi^{n'_{u'}*}_{q'_{u'}}(u')\Big(H_{\text{single,3D}}\Big)\sum_{\boldsymbol{q}} e^{-i\boldsymbol{q}\cdot\boldsymbol{r}_j}\prod_{u=x,y,z}\psi^{n_u}_{q_u}(u) \\ =& \sum_{\boldsymbol{q}\boldsymbol{q}'}\frac{E^n_{\boldsymbol{q}}}{L^6}e^{i\boldsymbol{q}'\cdot\boldsymbol{r}_i}e^{-i\boldsymbol{q}\cdot\boldsymbol{r}_j}\int \mathrm{d}\boldsymbol{r}\prod_{u'=x,y,z}\psi^{n'_{u'}*}_{q'_{u'}}(u')\prod_{u=x,y,z}\psi^{n_u}_{q_u}(u) \\ =& \sum_{\boldsymbol{q}\boldsymbol{q}'}\frac{E^n_{\boldsymbol{q}}}{L^6}e^{i\boldsymbol{q}'\cdot\boldsymbol{r}_i}e^{-i\boldsymbol{q}\cdot\boldsymbol{r}_j}\delta_{\boldsymbol{q}\boldsymbol{q}'}\delta_{nn'}L^3 \\ =& \frac{1}{L^3}\sum_{\boldsymbol{q}} E^n_{\boldsymbol{q}}e^{i\boldsymbol{q}\cdot(\boldsymbol{r}_i-\boldsymbol{r}_j)} \end{aligned} \tag{2.35}$$

We observe that there is no amplitude to go between states that are in two different bands, as is indicated by the appearance of $\delta_{nn'}$. In what follows, we will consider only the lowest band, $n = 0$, so we will drop the band index altogether. This simplification imposes two important requirements for our system:

1. **The temperature and the Fermi energy need to be small compared to the energy gap between the lowest and first excited band.**

2. **The interaction energy scale must also be small compared to the energy gap between the lowest and first excited band.**

In the 3D lattice, the total energy $E_{\boldsymbol{q}}$ is the sum of the energy associated with each quasimomentum component, $E_{\boldsymbol{q}} = \sum_{u=x,y,z} E_{q_u}$. By inserting this into the sum for t_{ij}

above we find

$$-t_{ij} = \frac{1}{L^3}\left[\left(\sum_{q_x} E_{q_x} e^{iq_x x_{ij}}\right)\sum_{q_y} e^{iq_y y_{ij}} \sum_{q_z} e^{iq_z z_{ij}} + \sum_{q_x} e^{iq_x x_{ij}}\left(\sum_{q_y} E_{q_y} e^{iq_y x_{ij}}\right)\sum_{q_z} e^{iq_z z_{ij}} + \sum_{q_x} e^{iq_x x_{ij}} \sum_{q_y} e^{iq_y y_{ij}}\left(\sum_{q_z} E_{q_z} e^{iq_z z_{ij}}\right)\right] \quad (2.36)$$

We make use of the identity $\sum_{q_u} e^{iq_u(u_i-u_j)} = L\delta_{u_i u_j}$ to obtain

$$-t_{ij} = \frac{1}{L}\left[\left(\sum_{q_x} E^{1D}_{q_x} e^{iq_x x_{ij}}\right)\delta_{y_i y_j}\delta_{z_i z_j} + \left(\sum_{q_y} E^{1D}_{q_y} e^{iq_y x_{ij}}\right)\delta_{x_i x_j}\delta_{z_i z_j} + \left(\sum_{q_z} E^{1D}_{q_z} e^{iq_z z_{ij}}\right)\delta_{x_i x_j}\delta_{y_i y_j}\right] \quad (2.37)$$

If $i = j$ we have

$$-t_{ii} = \frac{3}{L}\sum_{q} E_q \quad (2.38)$$

Since q runs over the L different values in the set $q \in \left\{\frac{2\pi u}{aL} \mid u \in \{0, 1, \ldots L-1\}\right\}$, $-t_{ii}$ is nothing more than the mean energy of the 3D energy band, which we will refer to as E_0, $-t_{ii} \equiv E_0$

If $i \neq j$, tunneling can only occur along one of the lattice directions as can be seen from the different Kronecker delta terms that show up in Eq. 2.37. In other words, for the simple cubic potential, diagonal tunneling events are second order processes. If we write the distance between sites i,j as Δ_{ij}, the tunneling matrix element simplifies to [3]

$$-t_{ij} = \frac{1}{L}\sum_{q} E_q e^{iq\Delta_{ij}} \quad (2.40)$$

In the tight-binding approximation, terms for which $|\Delta_{ij}| > a$ are neglected, and Δ_{ij} can only take the values $-a$ or a, where a is the lattice spacing. In this case we use $t_{ij} \equiv t$, where t is given by

$$-t = \frac{1}{L}\sum_{q} E_q e^{iqa} \quad (2.41)$$

[3] In this section we have used the Wannier states constructed as a sum of plane waves to obtain the tunneling matrix element. It can also be obtained directly from the Wannier states' wavefunctions:

$$-t_{ij} = \int \mathrm{d}\boldsymbol{r}\, w_i(\boldsymbol{r}) H_{\mathrm{single,3D}} w_j(\boldsymbol{r}) \quad (2.39)$$

Calculating the tunneling matrix element by computing the overlap integral of the Wannier wavefunctions is computationally more expensive than obtaining it as a sum over the energy eigenvalues.

We can then go ahead and write the second quantized form of H_0 in the tight-binding approximation

$$H_0 = E_0 \sum_i a_i^\dagger a_i - t \sum_{\langle ij \rangle} a_i^\dagger a_j \tag{2.42}$$

The first term in this expression is constant for a system with a conserved number of particles, since $\sum_i a_i^\dagger a_i = N$. Usually this energy offset is neglected, but when dealing with inhomogeneous systems which have a position dependent lattice depth it will be important to take it into account, as we will see later on.

We can go ahead and invert the Fourier series in Eq. 2.40 to obtain

$$E_q = -\sum_{\Delta_{ij}} t_{ij} e^{-iq\Delta_{ij}} \tag{2.43}$$

which in the tight-binding approximation reduces to

$$E_q = -2t \cos(qa) \tag{2.44}$$

This explicit form for the dispersion relation allows us to relate the bandwidth, $W_{1\mathrm{D}}$, to the tunneling matrix element as $W_{1\mathrm{D}} = 4t$, which in 3D becomes $W_{3\mathrm{D}} = 12t$.

It is useful to find out the range of lattice depths for which the tight-binding approximation is valid in the optical lattice potential. To do this we just need to look at the tunneling matrix elements for beyond nearest-neighbor tunneling, as shown in Fig. 2.7. For lattice depths $\gtrsim 5E_R$ we can safely ignore beyond nearest-neighbor tunneling, see also Fig. 2.10.

Yet another way of estimating the tunneling matrix element [66] is by using the relationship $t = W_{1\mathrm{D}}/4$, valid in the tight-binding limit, and obtaining the bandwidth from the known properties of the Mathieu functions, which are solutions to the Schrodinger equation in a 1D lattice. This yields the analytic result

$$t/E_r \simeq \frac{4}{\sqrt{\pi}} v_0^{3/4} \exp(-2\sqrt{v_0}) \tag{2.45}$$

where v_0 is the lattice depth in units of the recoil energy. The comparison between the result from Eq. 2.40 and Eq. 2.45 is shown in Fig. 2.8.

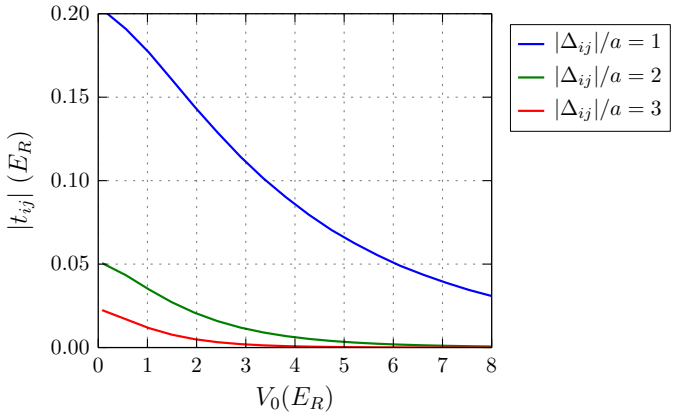

Figure 2.7: Tunneling matrix element in an optical lattice as a function of lattice depth. Nearest-neighbor and beyond nearest-neighbor matrix elements are shown to illustrate the range of lattice depths for which the tight-binding limit is a good approximation. Δ_{ij} corresponds to the distance between initial and final lattice sites in the tunneling matrix element.

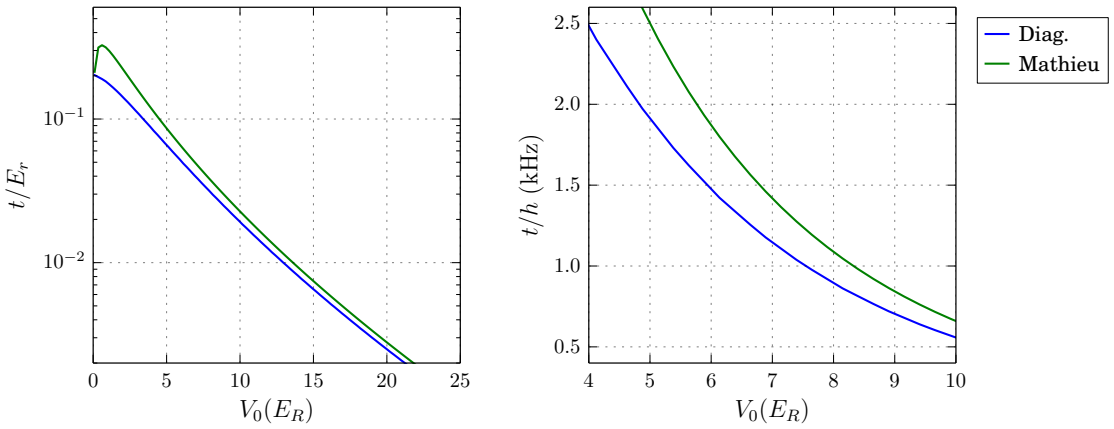

Figure 2.8: Nearest neighbor tunneling matrix element in an optical lattice as a function of lattice depth. Comparison between the result from Eq. 2.40 and the one obtained from the Mathieu functions, Eq. 2.45. The right panel shows the tunneling rate in kHz for the mass of a ^{6}Li atom.

Notice that, up to now, we have ignored the spin part of the wavefunction. We can include it easily by noticing that H_0 does not act on the spin at all, so the states $|i\rangle$ and $|j\rangle$ that we have used in the derivation above need to have the same spin. If two spin states are available, our basis set is twice as large, which can be taken care of by including a sum over spin states:

$$H_0 = E_0 N - t \sum_{\langle ij\rangle,\sigma=\uparrow\downarrow} a_{i\sigma}^\dagger a_{j\sigma} \tag{2.46}$$

On-site interaction energy, U. The interaction part of the hamiltonian for N particles is given by

$$H_{\text{int}} = \frac{1}{2} \sum_{l,m,l\neq m}^{N} V_{\text{int}}(\boldsymbol{r}_l, \boldsymbol{r}_m) \tag{2.47}$$

This is a two-particle operator, and its second quantized form is given by

$$H_{\text{int}} = \frac{1}{2} \sum_{i,j,k,m} \langle ij|V_{\text{int}}|km\rangle a_i^\dagger a_j^\dagger a_m a_k \tag{2.48}$$

where

$$\langle ij|V_{\text{int}}|km\rangle = \int \mathrm{d}\boldsymbol{r}_1 \int \mathrm{d}\boldsymbol{r}_2 \;\; \varphi_i^*(\boldsymbol{r}_1)\varphi_j^*(\boldsymbol{r}_2) V_{\text{int}}(\boldsymbol{r}_1, \boldsymbol{r}_2)\varphi_k(\boldsymbol{r}_1)\varphi_m(\boldsymbol{r}_2) \tag{2.49}$$

and the φ's correspond to the wavefunctions of the single particle basis states chosen.

The interaction between ultracold atoms can be described in terms of the s-wave scattering length, a_s, and a pseudo-potential [67, 66] given by[4]

$$V_{\text{int}}(\boldsymbol{r}_1, \boldsymbol{r}_2) = \frac{4\pi\hbar^2 a_s}{m} \delta(\boldsymbol{r}_1 - \boldsymbol{r}_2) \tag{2.50}$$

so the matrix element above can be written as

$$\langle ij|V_{\text{int}}|km\rangle = \frac{4\pi\hbar^2 a_s}{m} \int \mathrm{d}\boldsymbol{r} \;\; \varphi_i^*(\boldsymbol{r})\varphi_j^*(\boldsymbol{r})\varphi_k(\boldsymbol{r})\varphi_m(\boldsymbol{r}) \tag{2.51}$$

Our basis states, φ, are the 3D Wannier states defined in Eq. 2.13, which are separable in the three spatial coordinates. We recall that the Wannier states are labeled by the lattice

[4] This is a good approximation as long as the s-wave scattering lengths is small compared to the single-site harmonic oscillator length [68]. This condition is typically satisfied, and other concerns such as collisional losses or coupling to higher bands are significant before the s-wave scattering length becomes comparable to the harmonic oscillator length. The harmonic oscillator length in a lattice site is $\ell = a/(\pi v_0^{1/4})$, which for a $7\,E_r$ lattice with $a = 532\,\text{nm}$ is $\ell \approx 2000\,a_0$, where a_0 is the Bohr radius.

site around which they are centered, and by their band index. If we explicitly write out the two labels in the expression above, we obtain

$$\langle ij|V_{\text{int}}|km\rangle = \frac{4\pi\hbar^2 a}{m}\prod_{v=x,y,z}\int \mathrm{d}v \;\; w_i^{n_i}(v)w_j^{n_j}(v)w_k^{n_k}(v)w_m^{n_m}(v) \equiv U_{ijkm} \tag{2.52}$$

In general i, j, k, m can represent any lattice sites. We will restrict our treatment to on-site interactions by enforcing $i = j = k = m$, furthermore, we consider only Wannier states in the lowest band. With this considerations, and also explicitly writing down the spin quantum number, which so far was implicit in the indices $ijkm$, we find

$$H_{\text{int}} = \frac{U}{2}\sum_{\sigma\neq\sigma'}\sum_i a_{i\sigma}^\dagger a_{i\sigma'}^\dagger a_{i\sigma'}a_{i\sigma} \tag{2.53}$$

where we have defined $U \equiv U_{ijkm}$ for $i = j = k = m$. Within the single band approximation to the on-site interactions, we have

$$U/E_r = \frac{8}{\pi}\frac{a_s}{a}\prod_{v=x,y,z}\int w(v)^4\mathrm{d}v \tag{2.54}$$

Defining the number operator as $n_{i\sigma} = a_{i\sigma}^\dagger a_{i\sigma}$

$$\begin{aligned} H_{\text{int}} &= \frac{U}{2}\sum_{\sigma\neq\sigma'}\sum_i n_{i\sigma'}n_{i\sigma} \\ &= U\sum_i n_{i\uparrow}n_{i\downarrow} \end{aligned} \tag{2.55}$$

where i runs over all of the lattice sites.

To calculate the value of U we use the Wannier states obtained in Sec. 2.1.3. Alternatively, one can approximate the Wannier state by the Gaussian ground state in the local oscillator potential of one lattice site and carry out the integral analytically to obtain [66]

$$U = \sqrt{8\pi}\frac{a_s}{a}v_0^{3/4} \tag{2.56}$$

Figure 2.9 shows a comparison of the exact result and the Gaussian approximation to the Wannier state for a lattice with $\lambda = 1064\,\text{nm}$.

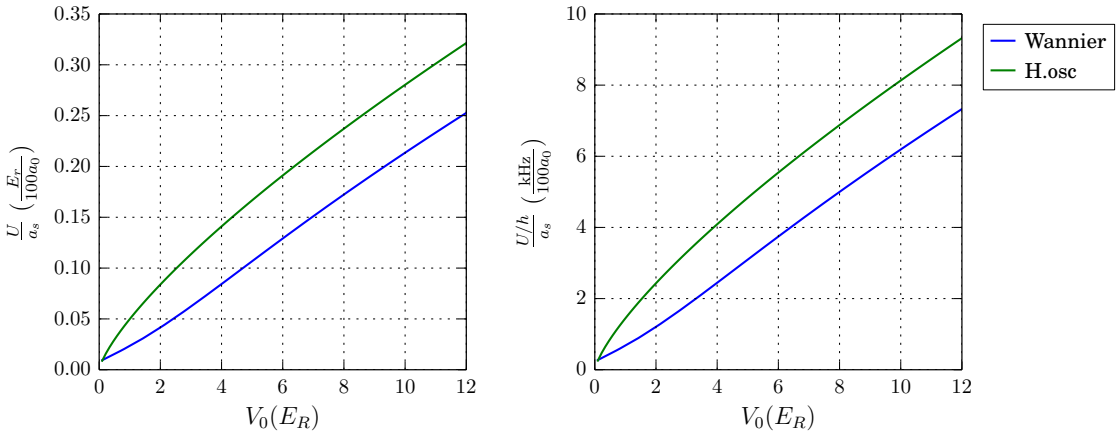

Figure 2.9: On-site interactions in a 3D lattice ($\lambda = 1064\,\text{nm}$) as a function of lattice depth. Numerical calculation using Wannier functions compared to the approximation using harmonic oscillator states. The lattice depth is the same in all three directions of the lattice. The left panel shows uses E_r for the units of U and the right panel uses kHz for U/h.

If the on-site interaction term is comparable to the energy spacing between the lowest and first excited bands, the single band approximation presented here breaks down. Corrections to the tunneling rate and the on-site interactions are necessary, which may depend on the lattice site occupation [69–71].

2.4 Parameter regimes for a valid description using a single band Hubbard model

Throughout this chapter we have mentioned the possible scenarios for which the single band Hubbard model is not an accurate description of ultracold atoms in an optical lattice. The two most important ones are:

- The on-site interaction U is comparable to the band gap Δ. The band gap is the energy difference between the highest energy state in the lowest band and the lowest energy state in the first excited band, see Fig. 2.6.

- Tunneling beyond nearest-neighbor (rate $t_2 \equiv t_{ij}$ for $\Delta_{ij} = 2a$, see Fig. 2.7) is not negligible compared to nearest-neighbor tunneling (rate t), i.e. the tight-binding approximation does not hold.

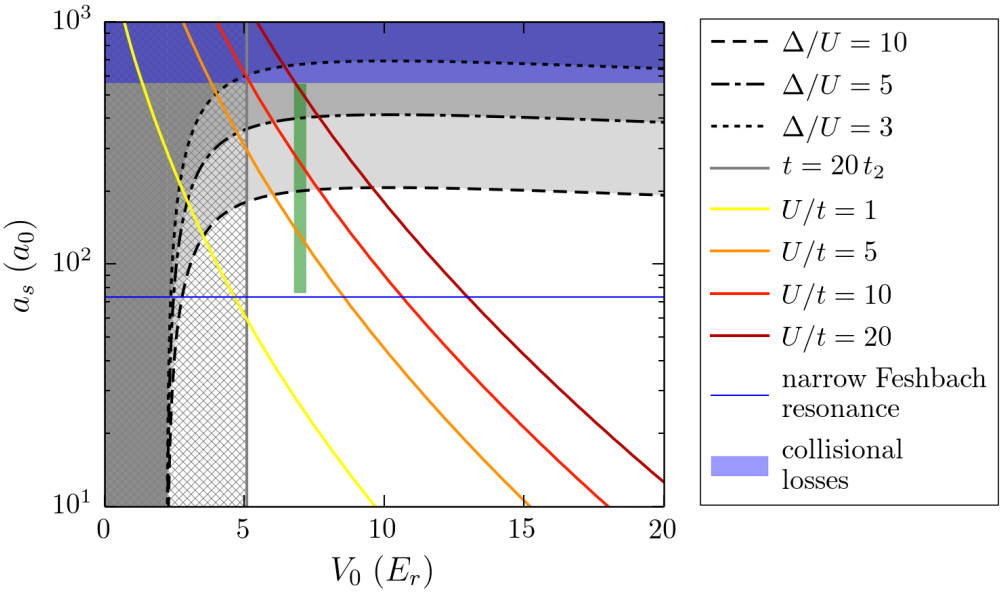

Figure 2.10: Regimes of validity for the single band Hubbard hamiltonian. The dashed black lines show curves at constant Δ/U. As U approaches Δ, higher bands have to be taken into account to describe the system accurately [69]. The vertical gray line indicates the lattice depth at which $t = 20t_2$, which delimits the region of validity of the tight-binding approximation. Yellow to brown hued lines indicated curves at constant U/t. The thin blue line indicates the background s-wave scattering length in the vicinity of the narrow Feshbach resonance of ^6Li [72, 73]. The shaded blue area indicates the range of scattering lengths over which we see significant collisional losses and heating of the sample. The shaded green area denotes the parameter regime covered by the experiments carried out in this thesis.

In Fig. 2.10 we have represented these two conditions as a function of the lattice depth and the s-wave scattering length. For more details on the validity of the single band Hubbard hamiltonian see Ref. [69].

Approximate solutions to the Hubbard model are explained, including the high-temperature series expansion (HTSE) which is widely used throughout this thesis.

3.1 Simplified treatments

This section explains our understanding of the Fermi-Hubbard model. It starts by building some insight by using the results of exactly solvable models. The results of exact diagonalization in systems of 2-sites and 4-sites are shown. This are going to motivate the antiferromagnetic character of the ground state, while showing that there is always a bit of an admixture of double occupancy in the exact ground state.

The 4-site solution can be used to help understand why the Fermi-Hubbard is relevant to high-Tc superconductors. In this case one can make connections to the d-wave character of ground states upon doping the system.

The exact diagonalization solutions are at zero temperature, so they give most insight to the exact ground states of the system.

3.1.1 Exact diagonalization

2 site exact diagonalization

4 site plaquette an relevance to high-Tc superconductors

3.1.2 Limiting cases

This section deals with the limiting cases of the Fermi-Hubbard parameters. The solutions that are obtained give insights to the workings of the model. The high temperature series expansion is introduced, which is very relevant for calculating thermodynamic quantities in the temperature regime of a few times T_{Neel}.

U=0 limit, t=0 limit

3.2 High-temperature series expansion

I will explain the derivation and results of the high temperature series expansion to second order in T/t.

3.3 Modern techniques

In this section I plant to give an outline of DQMC and NLCE.

Compensated optical lattice potential

This chapter will consist of the detailed report that I wrote on the use of the compensated optical lattice to control the density of the sample and enable evaporative cooling of the atoms in the lattice.

Experimental diagnostic tools

This chapter aims to describe in detail the different observables that are accessible to us, and describe in a general way the setups that we use to measure them.

Experimental setup and procedures

In this chapter I will go into details about the implementations of the methods in our particular setup. Details about calibrations and other details very specific to our experiment will be in this chapter.

6.1 Production of a deeply degenerate ^{6}Li spin mixture in a dimple potential

6.2 Compensated optical lattice potential, calibrations

6.3 Lattice loading

6.4 Round-trip temperature measurements

6.5 Bragg scattering setup

Mott insulating state in a simple cubic lattice

This chapter will contain the details of the paper on the incompressibility of the Mott insulator on which I am working at the moment.

Antiferromagnetic correlations in the Hubbard model

This chapter will contain the results of the AFM paper.

Conclusion

BIBLIOGRAPHY

[1] X. Wen, *Quantum Field Theory of Many-Body Systems: From the Origin of Sound to an Origin of Light and Electrons*, *Oxford Graduate Texts* (OUP Oxford, 2004).

[2] A. Altland and B. Simons, *Condensed Matter Field Theory* (Cambridge University Press, 2010).

[3] N. Ashcroft and N. Mermin, *Solid state physics* (Saunders College, 1976).

[4] L. Landau, *Collected papers of L. D. Landau* (Gordon and Breach, 1965).

[5] K. Andres, J. E. Graebner, and H. R. Ott, "$4f$-Virtual-Bound-State Formation in $CeAl_3$ at Low Temperatures," Phys. Rev. Lett. **35,** 1779–1782 (1975).

[6] F. Steglich, J. Aarts, C. D. Bredl, W. Lieke, D. Meschede, W. Franz, and H. Schäfer, "Superconductivity in the Presence of Strong Pauli Paramagnetism: $CeCu_2Si_2$," Phys. Rev. Lett. **43,** 1892–1896 (1979).

[7] D. C. Tsui, H. L. Stormer, and A. C. Gossard, "Two-Dimensional Magnetotransport in the Extreme Quantum Limit," Phys. Rev. Lett. **48,** 1559–1562 (1982).

[8] R. B. Laughlin, "Anomalous Quantum Hall Effect: An Incompressible Quantum Fluid with Fractionally Charged Excitations," Phys. Rev. Lett. **50,** 1395–1398 (1983).

[9] J. Bednorz and K. Müller, "Possible high-T_c superconductivity in the Ba-La-Cu-O system," Zeitschrift für Physik B Condensed Matter **64,** 189–193 (1986).

[10] P. Coleman, "Many Body Physics: Unfinished Revolution," in *International Conference on Theoretical Physics*, D. Iagolnitzer, V. Rivasseau, and J. Zinn-Justin, eds., (Birkhäuser Basel, 2004), pp. 559–580.

[11] P. W. Anderson, "More Is Different," Science **177,** 393–396 (1972).

[12] X. Wen, "Topological orders in rigid states," International Journal of Modern Physics B **04,** 239–271 (1990).

[13] J. A. Hertz, "Quantum critical phenomena," Phys. Rev. B **14,** 1165–1184 (1976).

[14] S. Sachdev, *Quantum Phase Transitions*, *Quantum Phase Transitions* (Cambridge University Press, 2011).

[15] "The Hubbard model at half a century," Nature Physics **9,** 523–523 (2013).

[16] J. Hubbard, "Electron Correlations in Narrow Energy Bands. III. An Improved Solution," Proceedings of the Royal Society of London. Series A, Mathematical and Physical Sciences **281,** pp. 401–419 (1964).

[17] J. Quintanilla and C. Hooley, "The strong-correlations puzzle," Physics World **22,** 32–37 (2009).

[18] D. Jaksch, C. Bruder, J. I. Cirac, C. W. Gardiner, and P. Zoller, "Cold Bosonic Atoms in Optical Lattices," Phys. Rev. Lett. **81,** 3108–3111 (1998).

[19] R. P. Feynman, "Simulating physics with computers," International journal of theoretical physics **21,** 467–488 (1982).

[20] M. Greiner, O. Mandel, T. Esslinger, T. Hänsch, and I. Bloch, "Quantum phase transition from a superfluid to a Mott insulator in a gas of ultracold atoms," Nature pp. 39–44 (2002).

[21] N. Gemelke, X. Zhang, C.-L. Hung, and C. Chin, "In situ observation of incompressible Mott-insulating domains in ultracold atomic gases.," Nature **460,** 995–8 (2009).

[22] K. Jiménez-García, R. L. Compton, Y.-J. Lin, W. D. Phillips, J. V. Porto, and I. B. Spielman, "Phases of a Two-Dimensional Bose Gas in an Optical Lattice," Physical Review Letters **105,** 110401 (2010).

[23] S. Trotzky, L. Pollet, F. Gerbier, U. Schnorrberger, I. Bloch, N. V. Prokof'ev, B. Svistunov, and M. Troyer, "Suppression of the critical temperature for superfluidity near the Mott transition," Nature Physics **6,** 998–1004 (2010).

[24] M. J. Mark, E. Haller, K. Lauber, J. G. Danzl, a. J. Daley, and H.-C. Nägerl, "Precision Measurements on a Tunable Mott Insulator of Ultracold Atoms," Physical Review Letters **107,** 175301 (2011).

[25] X. Zhang, C.-L. Hung, S.-K. Tung, and C. Chin, "Observation of quantum criticality with ultracold atoms in optical lattices.," Science (New York, N.Y.) **335,** 1070–2 (2012).

[26] J. K. Freericks and H. Monien, "Phase diagram of the Bose-Hubbard Model," EPL (Europhysics Letters) **26,** 545 (1994).

[27] W. Krauth and N. Trivedi, "Mott and Superfluid Transitions in a Strongly Interacting Lattice Boson System," EPL (Europhysics Letters) **14,** 627 (1991).

[28] M. P. A. Fisher, P. B. Weichman, G. Grinstein, and D. S. Fisher, "Boson localization and the superfluid-insulator transition," Phys. Rev. B **40,** 546–570 (1989).

[29] T. Fukuhara, P. Schauß, M. Endres, S. Hild, M. Cheneau, I. Bloch, and C. Gross, "Microscopic observation of magnon bound states and their dynamics.," Nature **502,** 76–9 (2013).

[30] D. Scalapino, "The case for $d_{x^2-y^2}$ pairing in the cuprate superconductors," Physics Reports **250,** 329 – 365 (1995).

[31] W. Hofstetter, J. I. Cirac, P. Zoller, E. Demler, and M. D. Lukin, "High-Temperature Superfluidity of Fermionic Atoms in Optical Lattices," Phys. Rev. Lett. **89,** 220407 (2002).

[32] Y.-R. Lee, M.-S. Heo, J.-H. Choi, T. T. Wang, C. A. Christensen, T. M. Rvachov, and W. Ketterle, "Compressibility of an ultracold Fermi gas with repulsive interactions," Phys. Rev. A **85,** 063615 (2012).

[33] M. Köhl, H. Moritz, T. Stöferle, K. Günter, and T. Esslinger, "Fermionic Atoms in a Three Dimensional Optical Lattice: Observing Fermi Surfaces, Dynamics, and Interactions," Physical Review Letters **94,** 080403 (2005).

[34] R. Jördens, N. Strohmaier, K. Günter, H. Moritz, and T. Esslinger, "A Mott insulator of fermionic atoms in an optical lattice.," Nature **455,** 204–7 (2008).

[35] U. Schneider, L. Hackermüller, S. Will, T. Best, I. Bloch, T. A. Costi, R. W. Helmes, D. Rasch, and A. Rosch, "Metallic and insulating phases of repulsively interacting fermions in a 3D optical lattice.," Science (New York, N.Y.) **322,** 1520–5 (2008).

[36] A. Damascelli, Z. Hussain, and Z. Shen, "Angle-resolved photoemission studies of the cuprate superconductors," Reviews of Modern Physics 75 (2003).

[37] R.-H. He *et al.*, "From a single-band metal to a high-temperature superconductor via two thermal phase transitions.," Science (New York, N.Y.) **331,** 1579–83 (2011).

[38] K. Jin, N. P. Butch, K. Kirshenbaum, J. Paglione, and R. L. Greene, "Link between spin fluctuations and electron pairing in copper oxide superconductors.," Nature **476,** 73–5 (2011).

[39] P. M. Grant, "High-temperature superconductivity: The great quantum conundrum.," Nature **476,** 37–9 (2011).

[40] E. Koch, in *Correlated Electrons: From Models to Materials*, E. Pavarini, E. Koch, F. Anders, and M. Jarrell, eds., (Forschungszentrum Jülich GmbH, Julich, Germany, 2012), Chap. 7. Exchange mechanisms.

[41] J. Milton, "Superconductors come of age,", Nature News. doi:10.1038/news.2010.527, 2010.

[42] M. K. Wu, J. R. Ashburn, C. J. Torng, P. H. Hor, R. L. Meng, L. Gao, Z. J. Huang, Y. Q. Wang, and C. W. Chu, "Superconductivity at 93 K in a new mixed-phase Y-Ba-Cu-O compound system at ambient pressure," Phys. Rev. Lett. **58,** 908–910 (1987).

[43] J. M. Tranquada *et al.*, "Antiferromagnetism in $YBa_2Cu_3O_{6+x}$," Phys. Rev. B **38,** 2477–2485 (1988).

[44] L. Liáng, *YBCO Superconductor Research Progress* (Nova Science Publishers, 2008).

[45] D. Greif, T. Uehlinger, G. Jotzu, L. Tarruell, and T. Esslinger, "Short-Range Quantum Magnetism of Ultracold Fermions in an Optical Lattice," Science 1307 (2013).

[46] S. Trotzky, P. Cheinet, S. Fölling, M. Feld, U. Schnorrberger, a. M. Rey, a. Polkovnikov, E. a. Demler, M. D. Lukin, and I. Bloch, "Time-resolved observation and control of superexchange interactions with ultracold atoms in optical lattices.," Science (New York, N.Y.) **319,** 295–9 (2008).

[47] S. Nascimbène, Y.-A. Chen, M. Atala, M. Aidelsburger, S. Trotzky, B. Paredes, and I. Bloch, "Experimental Realization of Plaquette Resonating Valence-Bond States with Ultracold Atoms in Optcal Superlattices," Phys. Rev. Lett. **108,** 205301 (2012).

[48] K. Kim, M.-S. Chang, S. Korenblit, R. Islam, E. Edwards, J. Freericks, G.-D. Lin, L.-M. Duan, and C. Monroe, "Quantum simulation of frustrated Ising spins with trapped ions," Nature **465,** 590–593 (2010).

[49] J. W. Britton, B. C. Sawyer, A. C. Keith, C.-C. J. Wang, J. K. Freericks, H. Uys, M. J. Biercuk, and J. J. Bollinger, "Engineered two-dimensional Ising interactions in a trapped-ion quantum simulator with hundreds of spins," Nature **484,** 489–492 (2012).

[50] J. Simon, W. S. Bakr, R. Ma, M. E. Tai, P. M. Preiss, and M. Greiner, "Quantum simulation of antiferromagnetic spin chains in an optical lattice," Nature **472,** 307–312 (2011).

[51] J. Struck, C. Ölschläger, R. Le Targat, P. Soltan-Panahi, A. Eckardt, M. Lewenstein, P. Windpassinger, and K. Sengstock, "Quantum Simulation of Frustrated Classical Magnetism in Triangular Optical Lattices," Science **333,** 996–999 (2011).

[52] F. Meinert, M. J. Mark, E. Kirilov, K. Lauber, P. Weinmann, A. J. Daley, and H.-C. Nägerl, "Quantum Quench in an Atomic One-Dimensional Ising Chain," Phys. Rev. Lett. **111,** 053003 (2013).

[53] P. Richerme, Z.-X. Gong, A. Lee, C. Senko, J. Smith, M. Foss-Feig, S. Michalakis, A. V. Gorshkov, and C. Monroe, "Non-local propagation of correlations in quantum systems with long-range interactions," Nature **511,** 198–201 (2014).

[54] T. Paiva, Y. L. Loh, M. Randeria, R. T. Scalettar, and N. Trivedi, "Fermions in 3D Optical Lattices: Cooling Protocol to Obtain Antiferromagnetism," Physical Review Letters **107,** 086401 (2011).

[55] S. Fuchs, E. Gull, L. Pollet, E. Burovski, E. Kozik, T. Pruschke, and M. Troyer, "Thermodynamics of the 3D Hubbard Model on Approaching the Néel Transition," Physical Review Letters **106,** 030401 (2011).

[56] D. C. McKay and B. DeMarco, "Cooling in strongly correlated optical lattices: prospects and challenges," Reports on Progress in Physics **74,** 054401 (2011).

[57] J. Imriška, M. Iazzi, L. Wang, E. Gull, D. Greif, T. Uehlinger, G. Jotzu, L. Tarruell, T. Esslinger, and M. Troyer, "Thermodynamics and Magnetic Properties of the Anisotropic 3D Hubbard Model," Phys. Rev. Lett. **112,** 115301 (2014).

[58] T. A. Corcovilos, S. K. Baur, J. M. Hitchcock, E. J. Mueller, and R. G. Hulet, "Detecting antiferromagnetism of atoms in an optical lattice via optical Bragg scattering," Phys. Rev. A **81,** 013415 (2010).

[59] M. Rigol, T. Bryant, and R. R. P. Singh, "Numerical Linked-Cluster Approach to Quantum Lattice Models," Phys. Rev. Lett. **97,** 187202 (2006).

[60] O. Morsch and M. Oberthaler, "Dynamics of Bose-Einstein condensates in optical lattices," Rev. Mod. Phys. **78,** 179–215 (2006).

[61] J. C. Slater, "A Soluble Problem in Energy Bands," Phys. Rev. **87,** 807–835 (1952).

[62] C. Salomon, G. Shlyapnikov, and L. Cugliandolo, *Many-Body Physics with Ultracold Gases: Lecture Notes of the Les Houches Summer School: Volume 94, July 2010*, *Lecture Notes of the Les Houches Summer School* (OUP Oxford, 2013).

[63] W. Kohn, "Analytic Properties of Bloch Waves and Wannier Functions," Physical Review **115,** 809–821 (1959).

[64] A. Fetter and J. Walecka, *Quantum Theory of Many-particle Systems*, *Dover Books on Physics* (Dover Publications, 2003).

[65] F. Schwabl, *Advanced Quantum Mechanics*, *Advanced texts in physics* (Springer, 2005).

[66] I. Bloch and W. Zwerger, "Many-body physics with ultracold gases," Reviews of Modern Physics **80,** 885–964 (2008).

[67] J. Sakurai and J. Napolitano, *Modern Quantum Mechanics* (Pearson Education, 2014), Chap. 6. Scattering theory.

[68] T. Busch, B. Englert, K. RzaÅijewski, and M. Wilkens, "Two cold atoms in a harmonic trap," Foundations of Physics pp. 549–559 (1998).

[69] F. Werner, O. Parcollet, A. Georges, and S. R. Hassan, "Interaction-Induced Adiabatic Cooling and Antiferromagnetism of Cold Fermions in Optical Lattices," Phys. Rev. Lett. **95,** 056401 (2005).

[70] R. Jördens, Ph.D. thesis, ETH Zürich, 2010.

[71] M. Mark, Ph.D. thesis, Innsbruck, 2012.

[72] K. E. Strecker, G. B. Partridge, and R. G. Hulet, "Conversion of an Atomic Fermi Gas to a Long-Lived Molecular Bose Gas," Phys. Rev. Lett. **91,** 080406 (2003).

[73] G. Zürn, T. Lompe, a. N. Wenz, S. Jochim, P. S. Julienne, and J. M. Hutson, "Precise Characterization of ^{6}Li Feshbach Resonances Using Trap-Sideband-Resolved RF Spectroscopy of Weakly Bound Molecules," Physical Review Letters **110,** 135301 (2013).